Communications Biology

https://doi.org/10.1038/s42003-026-09684-x

Article in Press

Pathological characteristics of SARS-CoV-2 variants and immune responses induced in a COVID-19 macaque model

Received: 21 November 2024

Accepted: 30 January 2026

Cite this article as: Urano, E., Okamura, T., Higuchi, M. *et al.* Pathological characteristics of SARS-CoV-2 variants and immune responses induced in a COVID-19 macaque model. *Commun Biol* (2026). https://doi.org/10.1038/s42003-026-09684-x

Emiko Urano, Tomotaka Okamura, Mahoko Higuchi, Mugi Furukawa, Kayoko Ueda, Satoshi Nagata, Haruhiko Kamada & Yasuhiro Yasutomi

Pathological characteristics of SARS-CoV-2 variants and immune responses induced in a COVID-19 macaque model

Emiko Urano[1], Tomotaka Okamura[1], Mahoko Higuchi[1], Mugi Furukawa[1], Kayoko Ueda[1], Satoshi Nagata[2], Haruhiko Kamada[3], Yasuhiro Yasutomi[1, 4, 5*]

[1] Laboratory of Immunoregulation and Vaccine Research, Tsukuba Primate Research Center, National Institutes of Biomedical Innovation, Health and Nutrition, Tsukuba, Ibaraki, Japan

[2] Laboratory of Antibody Design, National Institutes of Biomedical Innovation, Health and Nutrition, Osaka, Japan

[3] Center for Drug Design Research, National Institutes of Biomedical Innovation, Health and Nutrition, Osaka, Japan

[4] Institute for Vaccine Research and Development, Hokkaido University, Sapporo, Hokkaido, Japan

[5] Division of Immunoregulation, Department of Molecular and Experimental Medicine, Mie University Graduate School of Medicine, Tsu, Mie, Japan

* Corresponding author

Email: yasutomi@nibn.go.jp (YY)

Abstract

Although recent studies have suggested that the Omicron strain is less severe, the prevalence of long Omicron variants and their subvariant waves continues today. Here, we analyze the pathological characteristics of SARS-CoV-2 variants in cynomolgus macaques. Prolonged re-challenge analysis results in the establishment of re-infection in some macaques with both the same strain and different strains. Omicron infection shows low pathogenicity; however, all macaques that developed pneumonia were inoculated with Omicron strains at the second inoculation. Interestingly, antibodies against the Wuhan, Alpha, and Delta strains are strongly induced regardless of the strain, but antibodies against Omicron strains are not. Moreover, despite the re-infection strain, antibody levels against the Wuhan strain are highest, suggesting original antigenic sin. In addition, Omicron infection induces weaker antigen-specific T-cell responses. These results indicate that immune responses to viral infection differ between the variants, and these differences could inform vaccine development strategies.

Introduction

Since the World Health Organization (WHO) declared a pandemic status and the outbreak of severe acute respiratory syndrome coronavirus 2 (SARS-CoV-2) on March 11, 2020, the virus has continued to spread globally, leading to recurring waves of infection[1]. These waves are largely attributed to the frequent genetic mutations in the virus. The viral mutations are considered to be factors that greatly influence the outbreak, and each of them is referred to as a "variant of concern (VOC) ". Alpha, Beta, Gamma, Delta, and Omicron variants have become global threats.

It is well known that RNA viruses are unstable and frequently mutate, and this pandemic has reaffirmed that coronaviruses are no exception. The viral mutation is considered to be one of the major factors associated with outbreaks due to the potential for repeated re-infection of the virus. If re-infection with obvious clinical symptoms cannot be established, the transmission will likely end, but unfortunately, re-infection with SARS-CoV-2 continues. There were reports of re-infection during the early days of the Wuhan strain outbreak, but it was very rare and was mostly mild or asymptomatic[2, 3]. Re-challenging models of non-human primates (NHPs) have been reported, and protective immunity in NHPs infected with SARS-CoV-2 is induced against re-exposure in NHPs[2, 4]. In fact, we also reported that when NHPs that had recovered from the Wuhan strain infection were re-inoculated with the same strain of virus, infection was not observed [5]. However, re-infection with heterologous strains is not uncommon in mutant viruses, and as long as this situation continues, the end of infection cannot be expected. Indeed, when new variants emerged, such as the Omicron variant, re-infection and breakthrough infections became problematic [6, 7]. Given these facts, it is essential to understand the differences in characteristics among variants in virus replication, pathogenesis, and immune response for pandemic countermeasures. In the current situation in which infection is spreading widely, it is also considered essential to understand the pathogenesis of re-infection.

The strain that spread worldwide after the initial Wuhan strain was the Alpha strain, originally called the London strain in November 2020[8]. The Alpha strain spread around the world in a period of only a few months and replaced the Wuhan strain[9, 10]. The variants that emerged next, Beta and Gamma, were more endemic in South Africa and Brazil, respectively [11, 12]. The first Delta variant was reported in India in October 2020, and it then spread all over the world and completely replaced in 2021[13, 14]. It has been reported that this virus is highly infectious and causes many severe cases[15, 16, 17]. After the rapid spread of the Delta strain and its decline, the Omicron strain of SARS-CoV-2 emerged in November 2021[18]. It was found in humans and laboratory animals that the Omicron strain of SARS-CoV-2 is highly infectious but has tended to have low pathogenicity[19, 20, 21]. The Omicron strain of SARS-CoV-2 was initially a subspecies called BA.1, but BA.1 later changed to subspecies BA.2, BA.4, and BA.5, and their subvariants, BQ.1, XBB, and then JN.1 are currently prevalent[22, 23, 24, 25]. Several groups have demonstrated that the lower pathogenicity of Omicron variants compared to that of Delta variant in human and animal models[26, 27, 28, 29, 30]. However, comprehensive analysis of the differences in immune induction by natural infection and its relationship to re-infection is required. Most studies elucidated cross-reactivity against several variants, which were analyzed using peripheral blood samples from vaccinated and convalescent individuals[31, 32, 33, 34], with limited studies on re-infection and virus transmission using rodent model[35, 36]. Moreover, since most people around the world have already received several doses of the Wuhan and other types of vaccine, it is difficult to assess the differences in immunity induced by natural infection.

We have reported SARS-CoV-2 infected Cynomolgus monkeys (CMs) reflect human COVID-19 pathological condition and also described the usefulness of CMs for understanding various viral infection[5, 37, 38, 39]. In the present study, we analyzed the viral dynamics and pathology of SARS-CoV-2 VOCs from Wuhan to Omicron strains, using a COVID-19 CM model. Elucidating how

adaptive immunity is induced by SARS-CoV-2 natural infection is critical for establishing a vaccine strategy, serologic therapies, public health control, and infection prediction. Given the re-infection concerns described above, we conducted prolonged re-challenge analysis using the COVID-19 CM model re-inoculated with either the same strain of SARS-CoV-2 as that used for the initial infection or a different strain.

Results

Clinical symptoms in CMs infected with VOCs

The ancestor strain Wuhan and six variants of concern (VOCs) that emerged including Alpha, Beta, Gamma, Delta, Omicron BA.1 and BA.2, were examined using CMs in this study (Table 1). All of the CMs were infected with $1x10^6$ $TCID_{50}$ SARS-CoV-2 by the intratracheal (IT) route (Fig. 1A). Obvious clinical symptoms were not observed after SARS-CoV-2 infection, but the main causes of the increases in scores were decreased appetite and decreased bowel movement (Fig. 1B and Fig. S1A). Body temperature was monitored at the same time every day by an intraperitoneally embedded data logger, and CMs had a fever for 1-2 days after all VOC infections and body temperature was consistently high in Gamma-infected CMs (Fig. 1C and Fig. S1B). Unfortunately, body temperature of #069 could not be monitored due to logger failure. No significant body weight loss was observed in any of the CMs (Fig. 1D and Fig. S1C). Decreases in white blood cells (WBCs) and platelets (PLT) after infection were one of the common features of SARS-CoV-2 infection and well maintained among VOCs (Fig. 1E and 1F). The inflammatory biomedical marker C-reactive protein (CRP) was elevated in most CMs on day 2 but decreased rapidly on day 3 in all CM groups (Fig. 1G–H, Fig. S2C). Interestingly, CRP also tended to increase in Omicron-infected CMs, while Wuhan, Alpha, and Gamma variants showed significantly higher levels than BA.1 and BA.2 (Fig. 1H). Biomarkers of energy metabolism, including glucose, cholesterol, and triglycerides, were also monitored during infection; however, no notable changes were observed (Fig. S3). There were no apparent differences in common clinical symptoms in the CMs infected with the variants, but lower CRP suggested that the Omicron variants have lower inflammatory responses associated with viral infection.

Comparison of rates of virus replication in CMs infected with VOCs

Viral replication and shedding were monitored by swab RT-PCR and infectious viruses were

examined by measuring $TCID_{50}$ using VeroE6/TMPRSS2. A significantly higher peak viral load and a longer virus shedding period were observed in both nasal and pharyngeal swab samples from CMs inoculated with the Delta variant (Fig. 2 and Fig.S4A). Because the virus was inoculated only via the IT route, viral propagation in the lower respiratory tract, such as the lungs, should be more reflective, especially in pharyngeal swabs. Therefore, the viral detection rate in nasal swab samples varied among the VOCs, ranging from 100% in Delta-infected CMs to 0% in CMs infected with Omicron strains BA.1 and BA.2, suggesting a lower replication capacity of Omicron variants in the lungs (Fig. 2A, C, and D). In the pharyngeal swab samples, the peak viral load tended to increase from the Wuhan to the Delta strains, and then significantly decreased from the Delta to the BA.2 strains (Fig. 2B–D). Similar but clearer results were obtained when the infectious viruses were examined by measuring the TCID50 using the same nasal and pharyngeal swab samples (Fig. 2C–D). Consistent with the peak viral load results, the highest replication capacity of the Delta variant among the VOCs was confirmed by area under the curve (AUC) analysis from days 0 to 7 (Fig. 2D). Viral RNA was detected in rectal swabs from a few CMs (Fig. S4B).

Development of lung pneumonia in CMs infected with VOCs

Lung pneumonia was examined using computed tomography (CT) analysis. Representative 3D images of the most severe inflammation in the lungs are shown in Fig. 3A. No significant differences were observed in the area of peak lung inflammation (Fig. 3B). However, inflammation was consistently observed in CMs infected with Wuhan and early emerging variants (Fig. 3A). Most CMs infected with each variant developed pneumonia; however, lung pneumonia was not confirmed in some CMs. Animal lung images are shown at 5 days post-infection (dpi). Interestingly, a characteristic ground glass opacity (GGO) pattern was observed in CMs infected with early variants, including the Alpha, Beta, Gamma variants, and clear inflammatory images obtained in Delta-infected CMs if pneumonia had developed (Fig. 3A). In contrast, inflammatory

spots were faint in CMs infected with Omicron variants, especially BA.1. These results were consistent with the increasing CRP levels, as shown in Fig. 1G, and Omicron's lower viral replication capacity in the lower respiratory tract, such as the lungs, may reflect weaker pneumonia development.

Viral distribution in systemic organs and in the lungs

At least one of each variant-infected CM was subjected to pathological dissection at 7 to 14 dpi, and the results of RT-PCR for those CMs are shown in Fig. S5. Loads of the virus detected by RT-PCR in organs were measured by a previously reported method for assessing pharmaceutical products, including vaccines so that all individuals could be compared equally[5, 40]. As we previously observed in Wuhan-infected CMs, high levels of the viral N2 gene (Fig. S5A) and substantial amounts of sgRNA, indicative of live viruses (Fig. S5B), were detected mainly in the respiratory region at 7 dpi in SARS-CoV-2-infected CMs. Viral loads tended to be high in one each of the Gamma- and Delta-infected animals. At 14 days after infection, viral N2 gene levels were decreased and RNA-detected regions were more limited in the CMs (Fig. S5C). In addition, sgRNA was not detected in most tissues and organs at 14 dpi (data not shown), suggesting that live viruses were cleared *in vivo* by 14 dpi. Although the number of animals analyzed was limited, higher viral replication capacity *in vivo* by VOCs that emerged early was observed, and the results are in agreement with the swab RT-PCR results.

Re-exposure of the SARS-CoV-2-infected CMs to the same variant or different variants

Next, we investigated the occurrence of re-infection using VOCs. We previously have reported that re-infection of the Wuhan strain was not confirmed by swab RT-PCR in CMs initially infected with the same Wuhan strain[5]. Therefore, we investigated whether the same variant or a different variant is able to establish re-infection in SARS-CoV-2-infected CMs. CMs were re-exposed to $1x10^6$ $TCID_{50}$ of the same or a different virus strain by the IT route at 84 days post

initial infection (Fig. 4A). The set of virus strains used for the initial infection and second infection is shown in Table 2. In addition, CMs of advanced-age were tested since cytokine storm-like symptoms occurred in an aged monkey after the second exposure to the Wuhan strain in our previous study[5]. Considering the physical burden for elderly CMs, body temperature was not monitored by an intraperitoneally embedded data logger in elderly CMs. Due to the limited number of animals in the re-infection analysis and the combination of viral strains used in the initial and second infections, we have displayed the groups according to the strains used in the initial infection. Body temperature and the level of CRP transiently increased after re-infection in most of the CMs (Fig. 4B and 4C), and re-infection was determined by RT-PCR using pharynx swab samples (Fig. 4D). Since hyperglycemia is one of the reported manifestations of the post-acute sequelae of SARS-CoV-2 infection biomarkers of glucose metabolism were monitored in re-infected CMs during the experimental period; however, no significant differences were observed over time (Fig. S6). PCR positivity was confirmed in all of the CMs that were exposed to the Delta variant for a second time, even in same Delta strain re-infection. On the other hand, re-challenge with the Omicron strain showed results that were different to those for re-challenge with the Delta strain. When CMs were exposed to Omicron strains for a second time, half of the CMs were positive, and half of the CMs remained negative (Fig. 4D). These results might reflect the ability of viral propagation *in vivo* shown in Fig. 2 and Fig. S5**;** however, re-infection in 50% of the CMs was confirmed with re-exposure to Omicron strains despite their low replication capacity.

The pathological conditions of the lungs in re-challenged CMs were analyzed. Chest CT images were analyzed after the second inoculation of SARS-CoV-2, and inflammation images were seen in 4 of 12 animals (#058, #064, #070, and #071, Fig. S7A). CRP was tentatively increased in most animals after the second time of infection (Fig. 4C and S7B). Intriguingly, no pneumonia was observed after re-infection with the Delta strain, and all of the CMs that developed

pneumonia were inoculated with Omicron strains at the second inoculation and 2 of the 4 CMs, #070 and #071, were PCR-negative after the second inoculation (Fig. 4D). We previously reported that one CM of advanced aged developed pneumonia after the second Wuhan inoculation without detection of viral RNA in swabs and we found that cytokine storm-like cytokines elevation. Therefore, the serum levels of cytokines and chemokines were analyzed. In a previous study, levels of 24 of 29 measured cytokines and chemokines were increased in the serum of a Wuhan-re-injected CM with pneumonia. However, no elevation in storm-like cytokines and chemokines were observed either in animals that developed pneumonia or those that did not develop pneumonia in this study (data not shown). Only the levels of inflammatory cytokine IL-6 tended to be elevated in CMs that developed pneumonia after the second infection (Fig. S7C). On the other hand, viral N2 RNA was not detected in most tissues and organs at 7 days post-second infection in all CMs that developed pneumonia, suggesting that previous immune imprinting controlled a certain degree of virus propagation (Fig. S8).

Antibody responses in CMs re-exposed to SARS-CoV-2

Despite the low viral replication efficiency of Omicron variants, re-infection was also observed with Omicron variants, suggesting that Omicron is less immunogenic and that a single infection does not elicit a sufficient immune response to prevent re-infection. Antibodies (Abs) against the receptor binding domain (RBD) of each SARS-CoV-2 variant were examined by ELISA. When CMs were initially inoculated with the Wuhan or Delta variants, Abs against the RBDs of the Wuhan, Alpha, and Delta variants were well induced; subsequently, Ab levels were immediately increased after re-infection (Fig. 5A and S9). Levels of Abs against the Wuhan variant were most elevated after the second inoculation, at 91 dpi, of any viral strain (Fig. 5B), suggesting an “original antigenic sin”-like phenomenon by which the first antigenic variant encountered imprints life-long immunity[41, 42, 43]. In contrast, in CMs exposed to either of the Omicron variants for the first time,

most variant-specific RBD Abs were not clearly induced. Only Abs against BA.1 and BA.5 RBD were induced, albeit slowly, in Omicron-infected animals.

Interestingly, after the second infection, anti-Wuhan-RBD Abs were induced more strongly than were anti-Omicron-RBD Abs, even in second Omicron variants injection cases (#064, #066, #067, #070, and #071) (Fig. 5B). When the neutralizing activity was measured using a replication-competent live virus by a CPE-based luminometric assay, a certain level of neutralizing activity against BA.1, BA.2, and BA.5 was detected in plasma from Omicron-exposed CMs (Fig. S10). *In vitro* virus replication efficacy and syncytium formation ability are also lower for Omicron variants than for the Wuhan and Delta variants, and small amounts of neutralizing Abs (NAbs) might therefore be able to neutralize Omicron variants. Thus, we also analyzed neutralizing Abs in plasma by using a competition-based commercial kit, and a moderate level of NAb against BA.1 after the initial infection and boosted NAbs against VOCs that emerged early after the second infection were detected (Fig. S11). These results indicated that there is a difference in antigenicity between the VOCs that emerged early VOCs and Omicron variants.

T cell responses to SARS-CoV-2 in CMs infected with VOCs

Finally, we examined SARS-CoV-2-specific T-cell responses induced by SARS-CoV-2 infection using PBMCs at 70 dpi stimulated by Wuhan-spike, Delta-spike, Omicron BA.4/5-spike, and N-protein overlapping peptide pools (Fig. 6). In the re-challenge experiments, CMs were infected with four different viral strains, and the antigen-specific T-cell response was therefore analyzed by the group of viral strains that were used at the initial infection. Antigen-specific IFNγ^+ CD4$^+$ (Fig. 6A) and CD8$^+$ T cells (Fig. 6B) and CD107a$^+$ CD8$^+$ T cells (Fig. 6C) were measured, and the cells responded well to the spike peptides but showed a relatively weak response to the N pool peptide. Stimulation with the N-pool peptide yielded significantly fewer IFNγ^+ CD4$^+$ and CD107α^+ CD8$^+$ T cells than stimulation with Wuhan-spike peptide pools across the

group (Fig. 6 and Fig. S12). No significant tendency was observed in IFNγ$^+$ CD4$^+$ T cells among the spike pool peptides, but the number of IFNγ$^+$ CD4$^+$ T cells was slightly smaller in BA.1-infected CMs than in the other groups (Fig. 6A). Although a significant difference was not observed, interestingly, the number of IFNγ$^+$ CD8$^+$ T cells tended to be large under the condition of Wuhan-spike stimulation in all groups (Fig. 6B). Moreover, CD8$^+$ T cells in BA.1 and BA.2-infected groups showed a stronger response to the Wuhan-spike than to the BA4/5-spike of a subvariant of the same Omicron strain. In addition, the number of IFNγ$^+$ CD8$^+$ T cells was low in the BA.1 and BA.2-infected groups under the condition of other peptide stimulations. Similar results were obtained using isolated cells from the mediastinal lymph node (Fig. S12 B-C). Unlike the analyses using PBMCs, these analyses were performed after the second infection, as the lymph nodes were collected at the time of necropsy. Therefore, CD8$^+$ T cell responses to spike peptide pools were relatively higher in Omicron-infected CMs. No significant difference was observed between young and elderly CMs in the status of re-infection and immune response, possibly due to the limited number of animals.

Overall, although there was no significant difference due to the limited number of animals, antigen-specific T-cell responses induced by viral infection tended to be weaker in Omicron infections. These results are consistent with the antibody responses shown in Fig. 5 and indicate the lower immunogenicity of Omicron strains. This study using a COVID-19 CM model showed that PCR positivity occurred after re-infection with VOCs and that symptomatic infection occurred after re-infection with Omicron variants. These phenomena were presumably due to proliferative and immunogenic properties of the virus *in vivo*, and comparative studies of VOCs suggested that the immune responses induced by viral infection were different for the VOCs that emerged early and Omicron variants.

Discussion

Although COVID-19 countermeasures were established in an unprecedented manner in the history of vaccine development and therapeutic agents, further research and measures are clearly needed to improve the current situation and aid future preparedness. Animal models of human infectious diseases are important for elucidating disease pathogenesis and establishing vaccine strategies, serologic therapy, public health control, and infection prediction. Several NHP models have been used as suitable animal models to study SARS-CoV-2 due to their similarity in terms of COVID-19 symptoms[2, 44, 45, 46, 47]. We have established a CM model using young, healthy CMs and CMs of advanced age; the differences observed between the pathologies of young and elderly CMs are similar to those seen in humans[5, 38, 48]. In this study, we analyzed the dynamics and pathology of SARS-CoV-2 VOCs using a COVID-19 CM model.

No significant differences in the common clinical symptoms due to SARS-CoV-2 infection were observed among the variant-infected CM groups, as the SARS-CoV-2-infected CMs developed only mild symptoms. Unlike the increased glucose observed in the African green monkey study, hyperglycemia was not confirmed in this study, probably because most of the animals were monitored for 2 weeks, while glucose levels were highest at 4 weeks post-infection[49]. In contrast, pharyngeal swab RT-PCR results showed increased viral propagation from Wuhan to Delta variants, and significantly longer viral shedding was observed in Delta-infected CMs (Fig. 2). This result is consistent with the results of studies on the replication capacity of the Delta strain and indicates why the Delta variant quickly spread all over the world[17, 50, 51]. In contrast, the viral load in the pharyngeal swab samples began to decrease from the Delta variant to the BA.2 variant (Fig. 2B). All monkeys were inoculated with the virus via the IT route, indicating that the viral load in the pharyngeal swab samples reflected the viral replication capacity in the lower respiratory tract, such as the lungs. This is also consistent with the results of studies showing that the

replication capacity of the Omicron variants, especially in the lungs, was lower than that of the Delta variant; thus, the Omicron variants showed less virulence[52, 53, 54, 55]. Furthermore, comparative swab PCR results clearly demonstrate that the viral evolution strategy changed after the emergence of the Delta variant. At the beginning of the pandemic, it was suggested that viruses evolved to increase their replication capacity and transmissive ability to survive, and then shifted their strategy to evade the host immune system, although they lost some replication capacity once people became immune through vaccination. There have been few reports on characterization using a series of variants rather than comparatively specific variants, and the findings of this study may be useful for discussing the viral evolutionary process[33].

Early emerging variants showed higher CRP levels than Delta and Omicron (Fig. 1G–H), consistent with chest CT results. Pneumonia did not occur in any of the CMs infected with the Delta and Omicron-infected CMs; however, if pneumonia was confirmed, clear inflammation spots were observed in Delta-infected CMs (Fig. 3). In an independent unpublished study using the Delta variant, one aged animal was euthanized because of significant aggravation of various clinical symptoms. Overall, Delta infection exhibited obvious pathogenicity, whereas Omicron infection showed less virulence. The Gamma variant also showed high pathogenicity in body temperature changes, CRP elevation, and pneumonia. However, owing to the limited spread of infection, the Delta variant is a more suitable strain for pathological analysis and evaluation of antiviral treatments in *in vivo* studies. Indeed, the Delta variant was used to evaluate vaccines and therapeutics in several studies[56, 57, 58, 59].

Elucidating how patients' adaptive immunity is induced by natural SARS-CoV-2 infection is critical for establishing future vaccine strategies and public health control[60, 61]. Therefore, we conducted a prolonged re-challenge analysis using CMs that were re-inoculated with either the same strain of SARS-CoV-2 used for the initial infection or a different strain. Unlike the repeated

Wuhan strain injections, PCR again returned repeated positive results for Delta and BA.1 infections in some cases. Since the Delta variant showed the highest viral load in both pharyngeal and nasal swab samples, re-infection occurred because of its high replication capacity. However, lung pneumonia did not develop in any of the CMs after the second Delta infection, suggesting that viral propagation is controlled by the host immune system immediately after viral infection. However, despite the lower viral replication capacity of the Omicron variants, both PCR positivity and pneumonia were confirmed in CMs reinfected with the Omicron variants (Fig. S7A). Immunogenicity is correlated with the amount of the antigen; therefore, it is reasonable to assume that lower viral replication results in lower antigenicity. However, the induction of anti-Omicron RBD-specific Abs was poor, even after exposure to the Omicron variants twice (Fig. 5B). These results indicate that symptomatic re-infection was established only in Omicron-exposed CMs because of the low immunogenicity of Omicron variants. Interestingly, Abs against the RBDs of the ancestral Wuhan strain and variants that emerged early in the pandemic, including the Alpha, Gamma, and Delta variants, were strongly induced, regardless of the viral strain (Fig. 5). These results were consistent with those of a re-challenge study using Alpha and Beta strains and vaccine-induced immune cross-reactivity in a rhesus macaque model[62, 63, 64]. Similar results were obtained when neutralizing Abs were measured using a competition-based commercial kit: a moderate level of NAb against BA.1 was detected after the initial infection, and boosted NAbs against VOCs that emerged early were detected after the second infection (Fig. S11).

Original antigenic sin (OAS) is a concern for establishing vaccine strategies for rapidly evolving viruses such as the influenza viruses and SARS-CoV-2[65, 66, 67]. Recently, Schiepers et al. developed a system for measuring primary addiction by molecular fate-mapping of a serum antibody, and showed that primary Wuhan-spike immunization followed by BA.1-spike boosting induced substantial *de novo* antibody responses[68]. In contrast, a study comparing immune

responses in participants who had received the original mRNA boosters and those who had received Omicron-containing bivalent mRNA boosters of two vaccines showed only modest benefits to the bivalent mRNA vaccine, suggesting that immune imprinting of previous antigenic exposure may pose an issue[69, 70]. In addition, Ju et al. reported that BA.2 breakthrough infection after two or three vaccinations induced a certain level of cross-reactive immune responses against later Omicron subvariants; however, the OAS-like phenomenon greatly limits the improvement of variant-specific antibody responses[71]. In this study, OAS-like antibody responses were also observed after the second infection when CMs were infected with the Wuhan strain after the first infection (Fig. 5, #048, #058, and #045). In addition to antibody induction, SARS-CoV-2-specific T cell responses were weaker in Omicron-infected-CMs compared to those in Wuhan- and Delta-infected CMs (Fig. 6). However, after two exposures to Omicron, SARS-CoV-2-specific $CD8^+$ T cell responses were slightly increased, and the induced cellular immunity may have contributed to protection against later infection (Fig. S12). Previous reports investigating the immune responses in NHPs with prior infection or vaccination have also revealed the importance of both humoral and cellular immune responses in combating highly mutated SARS-CoV-2 variants[63, 72, 73, 74]. The number of animals was limited in our re-infection experiment; however, OAS-like phenomena pose a challenge to an effective immune response against newly emerged variants, and a lower T-cell responses induced by Omicron infection would be reasonable to discuss why we have a prolonged Omicron wave and the continuous emergence of its subvariants. Indeed, in humans, the Ab response did not change significantly before and after Omicron reinfection, and differential protection efficacy against reinfection was suggested between the pre- and post-Omicron eras[75, 76]. As a future vaccine strategy, a monovalent epidemic strain type of vaccine might be better because most of the world's population has been immunized with the immunogenic ancestor, the Wuhan-spike-based vaccine.

In this study, we determined these cross-reactive immune responses to viral challenge in naïve animals with various combinations of variants and observed differential cross-reactive immune induction. These findings on the inhomogeneous immunogenicity among variants are important for future vaccine strategies. Our study, using a series of VOCs, showed that COVID-19 CM models will clarify viral evolution and help devise effective vaccine strategies to combat the pandemic.

Materials and Methods

Viruses and cells. Wuhan strain (SARS-CoV-2/UT-NCGM02/Human/2020/Tokyo) and Omicron strains BA.1 (hCoV-19/Japan/NC928-2N/2021) and BA.2 (hCoV-19/Japan/UT-NCD1288-2N/2022), were provided by Professor Yoshihiro Kawaoka (The University of Tokyo). Alpha strain (QHN001), Beta strain (TY8-612), and Gamma strain (TY7-501) were provided by the National Institute of Infectious Diseases. Delta strain (TKYTK1734) and Omicron BA.5 (TKYTS14631) were provided by Tokyo Metropolitan Institute of Public Health. Viruses were propagated as previously described and used for the infection experiment[5]. Briefly, original stock viruses were propagated in Vero/TMPRSS2 cells cultured with 2% fetal bovine serum (FBS, Gibco) in DMEM medium at 37 °C for 3 days. The Omicron variants, BA.2 and BA.5, used for the rechallenge experiment were propagated in VeroE6/TMPRSS2 cells cultured with 2% FBS in DMEM medium at 37 °C for 2-3 days, and then the harvested culture supernatant was concentrated by centrifugation using Amicon Ultra-15 (Merck) according to the manufacturer's instructions. Vero/TMPRSS2 cells were obtained from JCRB Cell Bank and were maintained in 5% FBS DMEM supplemented with 1 mg/ml G418 (Roche). VeroE6/TMPRSS2 (P13) cells were obtained from JCRB Cell Bank and were maintained in 7% FBS DMEM supplemented with 1 mg/ml G418. All cells were cultured at 37 °C in a humidified 5% CO2 atmosphere. The tissue culture 50% infectious dose ($TCID_{50}$) of the virus was measured using VeroE6/TMPRSS2 cells.

Animals. Cynomolgus macaques (CMs, origin from Indonesia, Philippines, Malaysia and their and Cambodia's mixed) housed at the Tsukuba Primate Research Center (TPRC), National Institutes of Biomedical Innovation, Health and Nutrition (NIBN., Ibaraki, Japan) were used in this study after approval by the Committee on the Ethics of Animal Experiments of NIBN in accordance with the guidelines for animal experiments at NIBN (DSR01-36, -36R1, and -36R2). We have complied with all relevant ethical regulations for animal use. The CMs used in this

study are listed in Table 1 and Table 2. All of the animals were negative for B virus, SIV, STLV, and Mycobacterium. The animals were handled under the supervision of the veterinarians in charge of the animal facility. Animals were housed in adjoining individual primate cages, allowing them to make visual and auditory contact with one another for social interactions. The temperature was maintained at 25 ± 3 °C, with light for 12 h a 12-hour light cycle per day. The animals were given water ad libitum and fed daily with apples and a commercial monkey diet (Type CMK-2; Clea Japan, Inc.).

SARS-CoV-2 infection and sampling procedures. The animals were housed in animal biosafety level 3 (ABSL3) facilities at TPRC of NIBN during the experimental period and were monitored throughout the study for physical health and clinical assessment. The clinical status of CMs was scored daily in six categories: appearance (skin and fur; 0 - 10), secretion (nose, mouth, eyes; 0 - 5), respiration (0 - 15), discharging (feces and urine; 0-10), appetite (food intake; 0 - 10), and activity (0 - 15)[77]. Body temperature was monitored at the same time every day by an intraperitoneally embedded data logger (DST milli-HRT; Star-Oddi). Total twenty-eight cynomolgus macaques (Male 16, Female 12) were randomly divided into each group (Wuhan: n=5, Alpha: n=3, Beta: n=3, Gamma: n=3, Delta: n=6, BA.1: n=5, and BA.2: n=3). CMs were inoculated with SARS-CoV-2 under anesthesia in a BSL3 room via the intratracheal (1 ml) route with $1x10^6$ $TCID_{50}$ virus. Rechallenge experiments were performed with CMs listed in Table 2. Eight animals from the first infection experiment and four aged female animals were under the second re-infection experiment. CMs were re-exposed to $1x10^6$ $TCID_{50}$ virus intratracheally (1 ml) at 84 days after the initial infection. All animal experiments were conducted under anesthesia to obtain blood and swab samples and for CT scanning at each collection point. The euthanasia was performed following the acceptable method of euthanasia for non-human primates per the recommendations of the AVMA Guidelines for the Euthanasia of Animals. At euthanasia, under

intramuscular ketamine hydrochloride (7.5 mg/kg) anesthesia, the animals were deeply anesthetized via intravenous sodium pentobarbital administration (40-80 mg/kg) while confirming the eyelid reflex and respiration. Whole-blood samples were collected from the abdominal aorta and exsanguinated, then macaques were euthanized by overdose with an additional sodium pentobarbital (60-80 mg/kg), cardiac and respiratory arrest were confirmed, and then a necropsy was performed.

Microcomputed tomography (CT) imaging. CT images were obtained and analyzed as previously described[5]. Each animal was placed under anesthesia (7.5 mg/kg ketamine Hydrochloride and 3 mg/kg xylazine). CT images were obtained (80 kV, 400 CT μA, FOV: 160 mm, scan time: respiratory-gated 8 min). All CT scans were performed in a BSL3 facility using a 3D micro CT scanner system (Cosmo scan CT AX; Rigaku, Tokyo, Japan). After scanning, the lung images were reconstructed by using CosmoScan Database software of the micro-CT scanner (Rigaku Corporation, Japan). Slices of the third, sixth, and ninth thoracic vertebras, including the upper, middle, and lower lung areas, respectively, were selected. The images were analyzed by using a Cosmo scan CT viewer (Rigaku Corporation, Japan) and chest CT 3D images were analyzed by AZE Virtual Place (Canon).

RNA extraction and quantitative RT-PCR. Viral load in the swabs was measured as described previously[5]. Nasal, pharynx, and rectal swab samples were collected in 1 ml DMEM supplemented with 100 U/ml penicillin and 100 mg/ml streptomycin (Nacalai Tesque). According to the manufacturer's instructions, RNA was extracted from swab samples using a QiaAmp Viral RNA kit (QIAGEN). For the detection of viral RNA N2, 5 μl of extracted RNA was subjected to one-step real-time RT-PCR using a QunatiTect Probe RT-PCR (QIAGEN) kit on a QuantStudio3 (Applied Biosystems, Massachusetts, USA). The following primers and probe were used: forward primer 5'-AAATTTTGGGGACCAGGAAC-3' and reverse primer 5'-

TGGCAGCTGTGTAGGTCAAC-3' with probe FAM-5'-ATGTCGCGCATTGGCATGGA-3'-BHQ1. The reaction conditions of RT-PCR were 50°C for 30 minutes (reverse transcription) and 95°C for 15 minutes (activation of the polymerase), 45 cycles of 15 seconds at 95°C (denaturation) followed by 60 seconds at 60°C (annealing and extension).

Determination of the viral distribution *in vivo*. The viral distribution was examined and quantified at necropsy as previously described[5]. Samples were collected from the same place and the exact position of each lung lobe, tissues, and organs using a biopsy-punch instrument (5 mm; Kaijirushi, Tokyo, Japan). All of the samples collected from tissues and organs were placed in RNAlater solution (Invitrogen), and then each weight-scaled piece of a sample was subjected to RNA extraction. Tissue samples were homogenized by ZR BashingBead (ZYMO RESEARCH) with MagNA Lyser (Roche), and RNA was extracted using a Quick-RNA Miniprep Plus Kit (ZYMO RESEARCH). Real-time PCR was performed for viral RNA N2 and viral sgRNA. The N2 gene was amplified by the method described above. sgRNA was amplified using the following primers and probe: forward primer 5'-CGATCTCTTGTAGATCTGTTCTC-3' and reverse primer 5'-ATATTGCAGCAGTACGCACACA-3' with probe FAM-5'-ACACTAGCCATCCTTACTGCGCTTCG-3'-BHQ1. The reaction conditions of RT-PCR were 50°C for 30 minutes (reverse transcription) and 95°C for 15 minutes (activation of the polymerase), 45 cycles of 15 seconds at 95°C (denaturation) followed by 60 seconds at 60°C (annealing and extension).

Detection of anti-SARS-CoV-2 antibodies. Levels of SARS-CoV-2 receptor binding domain (RBD)-specific antibodies in plasma were measured by an enzyme-linked immunosorbent assay (ELISA) using purified RBD protein. RBDs (319–541 amino acids) of the spike proteins of wild-type of SARS-CoV-2 and its variants were produced as human IgG1 Fc-fusion proteins as described previously[5]. In brief, the coding sequences of spike proteins of Wuhan-Hu-1 strain

(NCBI Accession Number: YP_009724390.11), Alpha variant (GISAID ID: EPI_ISL_768526), Beta variant (EPI_ISL_1123289), Gamma variant (EPI_ISL_833366), Delta variant (EPI_ISL_2158617), BA.1 omicron variant (EPI_ISL_6640917), BA.2 omicron variant (EPI_ISL_ 9595859), and BA.5 omicron variant (EPI_ISL_13241867) were designed by codon optimization, synthesized, and subcloned into the pcDNA3.1 vector to generate fusion proteins with the Fc portion of human IgG1. For expression of the RBD-Fc-fusion proteins, the plasmids were transfected into Expi293F cells using the Expi293 Expression System (Thermo Fisher Scientific), and the cell culture supernatants were harvested. The produced RBD-Fc fusion proteins were purified by affinity chromatography using a Protein A HP column (Cytiva). A 96-well flat plate was coated with 100 μl of 0.1 μg/ml RBD-Fc overnight at 4°C and blocked with 1% BSA/PBS for 1 hour at 37°C. Plasma samples were inactivated by 1% Triton X-100 (Nacalai Tesque) and were placed at 1:100 dilutions in each well and incubated overnight at 4°C and then incubated with a 1:10000-diluted anti-Monkey IgG HRP (NORDIC IMMUNOLOGY, GAMON/IGG(H+L)/PO) for 1 hour at room temperature. The reaction was developed by adding a TMB substrate (Dako) and halted by adding a stop solution. The absorbance at 450 nm was read using by a GloMax (Promega). Assays were performed in triplicate in each experiment.

SARS-CoV-2 neutralization assay. Plasma was heat-inactivated by incubation at 56℃ for 30 min. Plasma samples at 1:10 dilutions were pre-incubated with equal amounts of 100 $TCID_{50}$ of SARS-CoV-2 viruses for 1 hour at room temperature, and then inoculated into VeroE6/TMPRSS2 cells in a 96-well plate and incubated for 1 hour at 37°C. Culture media were changed, and cells were incubated for the indicated time for each variant. Neutralization efficacy was examined by cell viability using CellTiter-Glo 2.0 (Promega), and the luminescent signal was read by GloMax (Promega). Non-heat-inactivated plasma samples were subjected to ProcartaPlex™ Human SARS-CoV-2 Variants Neutralizing Antibody Panel 6plex (Thermo Fisher Scientific).

Neutralizing antibodies towards SARS-CoV-2 S1, SARS-CoV-2 S1 B.1.1.529 (o), SARS-CoV-2 S1 B.1.1.7 (α), SARS-CoV-2 S1 B.1.351 (β), SARS-CoV-2 Spike B.1.617.2 P.1 (γ), and SARS-CoV-2 S1 B.1.617.2 (δ) were assessed according to the manufacturer's protocol. Beads were washed with 2% paraformaldehyde solution before reading, and then signals were detected and analyzed using a Luminex bio-plex system (Luminex, TX, USA) with Bio-Plex Manager 5.0 software (Luminex).

Serum biochemical analysis and cytokine and chemokine profiles. Cryopreserved serum was used for blood biochemical analysis as described previously[5]. The items (CRP: c-reactive protein; AST: aspartate aminotransferase; ALT: alanine aminotransferase; LDH: lactate dehydrogenase; ALP: alkaline phosphatase; BUN, blood urea nitrogen, GLU: glucose; T-CHO: total- cholesterol; and TG: triglycerides) were determined in a BSL3 laboratory by using the Fuji DRI-CHEM system (FUJIFILM, Tokyo, Japan), and IL-6 was determined in the BSL3 laboratory by using LUMIPULSE G600II (Fujirebio). The profiles of cytokines and chemokines in sera were analyzed using a cytokine monkey magnetic 29-plex panel for Luminex platform (Invitrogen, Thermo Fisher Scientific) according to the manufacturer's protocol. Beads were washed with 2% paraformaldehyde solution before reading, and then signals were detected and analyzed using a Luminex bio-plex system (Luminex, TX, USA) with Bio-Plex Manager 5.0 software (Luminex).

Intracellular cytokine staining. Antigen-specific cellular immune responses were assessed by multiple intracellular cytokine staining (ICS) assays. PBMCs were isolated from blood by density centrifugation using Lympholyte®-Mammal Cell Separation Media (Cerdarlane). Mediastinal lymph nodes were homogenized with the plunger, and cells were isolated by centrifuging in 0.5% FBS PBS. Cryopreserved PBMCs were thawed the day before antigen stimulation and cryopreserved mediastinal lymph node cells were thawed on the day of antigen stimulation, then cultured in R10 medium (RPMI 1640 with 2 mM L-glutamine, 100 U/ml

penicillin, 100 μg/ml streptomycin, 10% FBS, and 10 mM HEPES (Nacalai Tesque)) supplemented with 20 U/ml IL-2 (Shionogi) at 37°C. Then PBMCs and mediastinal lymph node cells were stimulated for 6 hr or 16 hr by adding approximately 0.1 ug of overlapping peptide pools (PepMix™ SARS-CoV-2 Wuhan spike: PM-WCPV-S-2, Delta spike: PM-SARS2-SMUT06-2, BA.4/BA.5 spike: PM-SARS2-SMUT10-2 (Innovative Peptide Solutions), and N protein: PepTivator® SARS-CoV-2 Prot_N (Miltenyi Biotch). At the same time, anti-CD107a (clone H4A3, BV605, BioLegend) Ab was added to the culture. Golgi Stop (BD) and Golgi Plug (BD) were added 2 hr after peptide stimulation at a final concentration of 0.7 μl/ml and 1 μl/ml respectively. For immunostaining analysis, cells were washed with 20 ug/ml DNase I (Roche) containing PBS, and then dead cells were stained with LIVE/DEAD Fixable Near-IR Dead Cell Stain (Life Technologies, Carlsbad, CA). The following monoclonal Abs were used for staining of cell surface markers at a 1:100 dilution: anti-CD3 (clone SP34-2, BUV395, BD #564117), anti-CD4 (clone OKT4, BV650, BioLegend #317436), and anti-CD8 (clone SK1, BUV496, BD OptiBuild #741199). ICS was performed using a BD Cytofix/Cytoperm™ Fixation/Permeabilization Kit (BD) and the following monoclonal Abs at a 1.5:100 dilution: anti-IFNγ (clone 4S.B3, PE, BD Pharmingen #559326), anti-IL-2 (clone MQ1-17H12, PerCP-Cy5.5, BD Pharmingen #560708, and anti-TNFa (clone Mab11, BV785, BioLegend #502948). Flow cytometric data were acquired using a FACS LSRFortessa X-20 flow cytometer (BD) and analyzed using FlowJo (BD) software. The intracellular cytokine-positive population under stimulation was calculated by subtracting the solvent control values.

Statistics and Reproducibility. Statistical analyses were performed using GraphPad PRISM software (version 9 and 10) and <0.05 was considered significant. Comparisons among groups were analyzed using one-way analysis of variance (ANOVA) followed by the Kruskal-Wallis test or two-way ANOVA with multiple comparison test. Due to the small number of animals (n=3-

6), statistical analysis was performed using non-parametric methods.

Supplementary information captions

Figures S1 to S13

Data and materials availability

All data associated with this study are in the paper or the Supplementary Materials and Supplementary Data 1 -3. The data that support the findings of this study are available from the corresponding author upon reasonable request.

Acknowledgments

We thank the members and veterinary staff of HAMRI Co., Ltd. and the Corporation for Production and Research of Laboratory Primates for their technical expertise and assistance with animal care and sample processing using cynomolgus macaques. This work was supported by the Japan Agency for Medical Research and Development (AMED), Research Program on Emerging and Re-emerging Infectious Diseases under JP20fk0108414 (to E.U., T.O., Y.Y.), JP21fk0108582 (to E.U.), by the AMED Strategic Center of Biomedical Advanced Vaccine Research and Development for Preparedness and Response (SCARDA), Japan Initiative for World-leading Vaccine Research and Development Centers under JP223fa627007 (to E.U., T.O., Y.Y.), JP223fa727002 (to Y.Y.), JP223fa627005 (to Y.Y.), by the Japan Society for the Promotion of Science (JSPS), KAKENHI Grant-in-Aid for Exploratory Research under 21K19395 (to E.U. and Y.Y.), by the Japan Science and Technology Agency (JST), under JPMJPF2017 (to Y.Y.). We would like to thank S.E.S. Translation and Proofreading Services and Editage (www.editage.jp) for English language editing.

Author Contributions

E.U. and Y.Y. designed the experiments. E.U., M.H., M.F., and K.U. performed the virological and the biological assays. T.O. analyzed CT images and veterinary pathology. S.N. and H.K. performed gene cloning and protein purification. E.U. and Y.Y. wrote the manuscript and all authors reviewed the manuscript.

Competing interests

The authors declare no competing interests.

References

1. Organization WH. Coronavirus disease (COVID-19) Weekly Epidemiological Updates and Monthly Operational Updates. (2023).

2. Chandrashekar A, *et al.* SARS-CoV-2 infection protects against rechallenge in rhesus macaques. *Science* **369**, 812-817 (2020).

3. Facciuolo A, *et al.* Longitudinal analysis of SARS-CoV-2 reinfection reveals distinct kinetics and emergence of cross-neutralizing antibodies to variants of concern. *Front Microbiol* **14**, 1148255 (2023).

4. Deng W, *et al.* Primary exposure to SARS-CoV-2 protects against reinfection in rhesus macaques. *Science* **369**, 818-823 (2020).

5. Urano E, *et al.* COVID-19 cynomolgus macaque model reflecting human COVID-19 pathological conditions. *Proc Natl Acad Sci U S A* **118**, (2021).

6. Kuhlmann C, *et al.* Breakthrough infections with SARS-CoV-2 omicron despite mRNA vaccine booster dose. *Lancet* **399**, 625-626 (2022).

7. Cele S, *et al.* Omicron extensively but incompletely escapes Pfizer BNT162b2 neutralization. *Nature* **602**, 654-656 (2022).

8. England PH. Investigation of novel SARS-COV-2 variant: Variant of Concern 202012/01. (2020).

9. Davies NG, *et al.* Estimated transmissibility and impact of SARS-CoV-2 lineage B.1.1.7 in England. *Science* **372**, (2021).

10. Davies NG, Jarvis CI, Edmunds WJ, Jewell NP, Diaz-Ordaz K, Keogh RH. Increased mortality in community-tested cases of SARS-CoV-2 lineage B.1.1.7. *Nature* **593**, 270-274 (2021).

11. Tegally H, *et al.* Detection of a SARS-CoV-2 variant of concern in South Africa. *Nature* **592**, 438-443 (2021).

12. Faria NR, *et al.* Genomics and epidemiology of the P.1 SARS-CoV-2 lineage in Manaus, Brazil.

Science **372**, 815-821 (2021).

13. Singh J, Rahman SA, Ehtesham NZ, Hira S, Hasnain SE. SARS-CoV-2 variants of concern are emerging in India. *Nat Med* **27**, 1131-1133 (2021).

14. Dhar MS*, et al.* Genomic characterization and epidemiology of an emerging SARS-CoV-2 variant in Delhi, India. *Science* **374**, 995-999 (2021).

15. Twohig KA*, et al.* Hospital admission and emergency care attendance risk for SARS-CoV-2 delta (B.1.617.2) compared with alpha (B.1.1.7) variants of concern: a cohort study. *Lancet Infect Dis* **22**, 35-42 (2022).

16. Deng X*, et al.* Transmission, infectivity, and neutralization of a spike L452R SARS-CoV-2 variant. *Cell* **184**, 3426-3437.e3428 (2021).

17. Saito A*, et al.* Enhanced fusogenicity and pathogenicity of SARS-CoV-2 Delta P681R mutation. *Nature* **602**, 300-306 (2022).

18. Viana R*, et al.* Rapid epidemic expansion of the SARS-CoV-2 Omicron variant in southern Africa. *Nature* **603**, 679-686 (2022).

19. Lewnard JA, Hong VX, Patel MM, Kahn R, Lipsitch M, Tartof SY. Clinical outcomes associated with SARS-CoV-2 Omicron (B.1.1.529) variant and BA.1/BA.1.1 or BA.2 subvariant infection in Southern California. *Nat Med* **28**, 1933-1943 (2022).

20. Meng B*, et al.* Altered TMPRSS2 usage by SARS-CoV-2 Omicron impacts infectivity and fusogenicity. *Nature* **603**, 706-714 (2022).

21. Halfmann PJ*, et al.* SARS-CoV-2 Omicron virus causes attenuated disease in mice and hamsters. *Nature* **603**, 687-692 (2022).

22. Organization WH. Updated working definitions and primary actions for SARS-CoV-2 variants, 4 October 2023.

23. Imai M*, et al.* Efficacy of Antiviral Agents against Omicron Subvariants BQ.1.1 and XBB. *N Engl J Med* **388**, 89-91 (2023).

24. Tegally H, *et al.* Emergence of SARS-CoV-2 Omicron lineages BA.4 and BA.5 in South Africa. *Nat Med* **28**, 1785-1790 (2022).

25. Yang S, *et al.* Fast evolution of SARS-CoV-2 BA.2.86 to JN.1 under heavy immune pressure. *Lancet Infect Dis* **24**, e70-e72 (2024).

26. Radhakrishnan N, *et al.* Comparison of the clinical characteristics of SARS-CoV-2 Delta (B.1.617.2) and Omicron (B.1.1.529) infected patients from a single hospitalist service. *BMC Infect Dis* **23**, 747 (2023).

27. Uraki R, *et al.* Characterization of SARS-CoV-2 Omicron BA.4 and BA.5 isolates in rodents. *Nature* **612**, 540-545 (2022).

28. Uraki R, *et al.* Characterization of SARS-CoV-2 Omicron BA.2.75 clinical isolates. *Nat Commun* **14**, 1620 (2023).

29. Mohandas S, *et al.* Comparative pathogenicity of BA.2.12, BA.5.2 and XBB.1 with the Delta variant in Syrian hamsters. *Front Microbiol* **14**, 1183763 (2023).

30. Martins M, *et al.* The Omicron Variant BA.1.1 Presents a Lower Pathogenicity than B.1 D614G and Delta Variants in a Feline Model of SARS-CoV-2 Infection. *J Virol* **96**, e0096122 (2022).

31. Chen RE, *et al.* Resistance of SARS-CoV-2 variants to neutralization by monoclonal and serum-derived polyclonal antibodies. *Nat Med* **27**, 717-726 (2021).

32. Wang Q, *et al.* Alarming antibody evasion properties of rising SARS-CoV-2 BQ and XBB subvariants. *Cell* **186**, 279-286.e278 (2023).

33. Reynolds CJ, *et al.* Immune boosting by B.1.1.529 (Omicron) depends on previous SARS-CoV-2 exposure. *Science* **377**, eabq1841 (2022).

34. Liu C, *et al.* Reduced neutralization of SARS-CoV-2 B.1.617 by vaccine and convalescent serum. *Cell* **184**, 4220-4236.e4213 (2021).

35. Halfmann PJ, *et al.* Transmission and re-infection of Omicron variant XBB.1.5 in hamsters.

EBioMedicine **93**, 104677 (2023).

36. Zhou J*, et al.* Omicron breakthrough infections in vaccinated or previously infected hamsters. *Proc Natl Acad Sci U S A* **120**, e2308655120 (2023).

37. Okamura T, Tsujimura Y, Soma S, Takahashi I, Matsuo K, Yasutomi Y. Simian immunodeficiency virus SIVmac239 infection and simian human immunodeficiency virus SHIV89.6P infection result in progression to AIDS in cynomolgus macaques of Asian origin. *J Gen Virol* **97**, 3413-3426 (2016).

38. Urano E, Okamura T, Kamitani W, Kawaoka Y, Yasutomi Y. Comparison of young and elderly COVID-19 cynomolgus macaque models reflecting human COVID-19 pathological conditions. *Translational and Regulatory Sciences* **4**, 20-24 (2021).

39. Urano E*, et al.* Establishment of a Cynomolgus Macaque Model of Human T-Cell Leukemia Virus Type 1 (HTLV-1) Infection by Direct Inoculation of Adult T-Cell Leukemia Patient-Derived Cell Lines for HTLV-1 Infection. *J Virol* **96**, e0133922 (2022).

40. Tsujimura Y*, et al.* Vaccination with Intradermal Bacillus Calmette–Guérin Provides Robust Protection against Extrapulmonary Tuberculosis but Not Pulmonary Infection in Cynomolgus Macaques. *The Journal of Immunology* **205**, 3023-3036 (2020).

41. Francis T. On the Doctrine of Original Antigenic Sin. *Proceedings of the American Philosophical Society* **104**, 572-578 (1960).

42. Fazekas de St G, Webster RG. Disquisitions of Original Antigenic Sin. I. Evidence in man. *J Exp Med* **124**, 331-345 (1966).

43. Fazekas de St G, Webster RG. Disquisitions on Original Antigenic Sin. II. Proof in lower creatures. *J Exp Med* **124**, 347-361 (1966).

44. Munster VJ*, et al.* Respiratory disease in rhesus macaques inoculated with SARS-CoV-2. *Nature* **585**, 268-272 (2020).

45. Yu P*, et al.* Age-related rhesus macaque models of COVID-19. *Animal Model Exp Med* **3**, 93-97 (2020).

46. Hartman AL, *et al.* SARS-CoV-2 infection of African green monkeys results in mild respiratory disease discernible by PET/CT imaging and shedding of infectious virus from both respiratory and gastrointestinal tracts. *PLOS Pathogens* **16**, e1008903 (2020).

47. Blair RV, *et al.* Acute Respiratory Distress in Aged, SARS-CoV-2-Infected African Green Monkeys but Not Rhesus Macaques. *Am J Pathol* **191**, 274-282 (2021).

48. Killingley B, *et al.* Safety, tolerability and viral kinetics during SARS-CoV-2 human challenge in young adults. *Nat Med* **28**, 1031-1041 (2022).

49. Palmer CS, *et al.* Non-human primate model of long-COVID identifies immune associates of hyperglycemia. *Nat Commun* **15**, 6664 (2024).

50. Mlcochova P, *et al.* SARS-CoV-2 B.1.617.2 Delta variant replication and immune evasion. *Nature* **599**, 114-119 (2021).

51. Zhang J, *et al.* Membrane fusion and immune evasion by the spike protein of SARS-CoV-2 Delta variant. *Science* **374**, 1353-1360 (2021).

52. Shuai H, *et al.* Attenuated replication and pathogenicity of SARS-CoV-2 B.1.1.529 Omicron. *Nature* **603**, 693-699 (2022).

53. Hui KPY, *et al.* SARS-CoV-2 Omicron variant replication in human bronchus and lung ex vivo. *Nature* **603**, 715-720 (2022).

54. Trunfio M, *et al.* Real-life Evidence of Lower Lung Virulence in COVID-19 Inpatients Infected with SARS-CoV-2 Omicron Variant Compared to Wild-Type and Delta SARS-CoV-2 Pneumonia. *Lung* **200**, 573-577 (2022).

55. van Doremalen N, *et al.* SARS-CoV-2 Omicron BA.1 and BA.2 are attenuated in rhesus macaques as compared to Delta. *Sci Adv* **8**, eade1860 (2022).

56. Jacob-Dolan C, *et al.* Immunogenicity and protective efficacy of GBP510/AS03 vaccine against SARS-CoV-2 delta challenge in rhesus macaques. *NPJ Vaccines* **8**, 23 (2023).

57. Urano E, *et al.* An inhaled ACE2 decoy confers protection against SARS-CoV-2 infection in preclinical models. *Sci Transl Med* **15**, eadi2623 (2023).

58. Rosenke K, *et al.* Combined molnupiravir-nirmatrelvir treatment improves the inhibitory effect on SARS-CoV-2 in macaques. *JCI Insight* **8**, (2023).

59. Gagne M, *et al.* Protection from SARS-CoV-2 Delta one year after mRNA-1273 vaccination in rhesus macaques coincides with anamnestic antibody response in the lung. *Cell* **185**, 113-130.e115 (2022).

60. Sette A, Crotty S. Adaptive immunity to SARS-CoV-2 and COVID-19. *Cell* **184**, 861-880 (2021).

61. Cromer D, *et al.* Prospects for durable immune control of SARS-CoV-2 and prevention of reinfection. *Nat Rev Immunol* **21**, 395-404 (2021).

62. Chandrashekar A, *et al.* Prior infection with SARS-CoV-2 WA1/2020 partially protects rhesus macaques against reinfection with B.1.1.7 and B.1.351 variants. *Sci Transl Med* **13**, eabj2641 (2021).

63. Chandrashekar A, *et al.* Vaccine protection against the SARS-CoV-2 Omicron variant in macaques. *Cell* **185**, 1549-1555.e1511 (2022).

64. Deng W, *et al.* Sequential immunizations confer cross-protection against variants of SARS-CoV-2, including Omicron in Rhesus macaques. *Signal Transduct Target Ther* **7**, 124 (2022).

65. Monto AS, Malosh RE, Petrie JG, Martin ET. The Doctrine of Original Antigenic Sin: Separating Good From Evil. *J Infect Dis* **215**, 1782-1788 (2017).

66. Henry C, Palm AE, Krammer F, Wilson PC. From Original Antigenic Sin to the Universal Influenza Virus Vaccine. *Trends Immunol* **39**, 70-79 (2018).

67. Evans JP, Liu SL. Challenges and Prospects in Developing Future SARS-CoV-2 Vaccines: Overcoming Original Antigenic Sin and Inducing Broadly Neutralizing Antibodies. *J Immunol* **211**, 1459-1467 (2023).

68. Schiepers A, *et al.* Molecular fate-mapping of serum antibody responses to repeat immunization.

Nature **615**, 482-489 (2023).

69. Collier AY, *et al.* Immunogenicity of BA.5 Bivalent mRNA Vaccine Boosters. *N Engl J Med* **388**, 565-567 (2023).

70. Wang Q, *et al.* Antibody Response to Omicron BA.4-BA.5 Bivalent Booster. *N Engl J Med* **388**, 567-569 (2023).

71. Ju B, *et al.* Antigenic sin of wild-type SARS-CoV-2 vaccine shapes poor cross-neutralization of BA.4/5/2.75 subvariants in BA.2 breakthrough infections. *Nat Commun* **13**, 7120 (2022).

72. Nelson CE, *et al.* Mild SARS-CoV-2 infection in rhesus macaques is associated with viral control prior to antigen-specific T cell responses in tissues. *Sci Immunol*, eabo0535 (2022).

73. Yu J, *et al.* Ad26.COV2.S and SARS-CoV-2 spike protein ferritin nanoparticle vaccine protect against SARS-CoV-2 Omicron BA.5 challenge in macaques. *Cell Rep Med* **4**, 101018 (2023).

74. Gagne M, *et al.* mRNA-1273 or mRNA-Omicron boost in vaccinated macaques elicits similar B cell expansion, neutralizing responses, and protection from Omicron. *Cell* **185**, 1556-1571.e1518 (2022).

75. Li L, *et al.* Immune response and severity of Omicron BA.5 reinfection among individuals previously infected with different SARS-CoV-2 variants. *Front Cell Infect Microbiol* **13**, 1277880 (2023).

76. Chemaitelly H, *et al.* Differential protection against SARS-CoV-2 reinfection pre- and post-Omicron. *Nature* **639**, 1024-1031 (2025).

77. Brining DL, Mattoon, J. S., Kercher, L., LaCasse, R. A., Safronetz, D., Feldmann, H., & Parnell, M. J. Thoracic Radiography as a Refinement Methodology for the Study of H1N1 Influenza in Cynomologus Macaques (Macaca fascicularis). *Comp Med*, (2010).

Figure legend

Figure 1. Study design and clinical signs in SARS-CoV-2-infected cynomolgus macaques. (A) Experimental regimens and timing of infection and necropsy. A total of twenty-eight cynomolgus macaques were intratracheally infected with $1x10^6$ TCID50 virus and red dots indicate the sampling time point (Wuhan: n=5, Alpha: n=3, Beta: n=3, Gamma: n=3, Delta: n=6, BA.1: n=5, and BA.2: n=3). (B) SARS-CoV-2-infected animals were monitored for clinical signs and were individually scored daily in six categories: appearance, secretion, respiration, discharging, appetite, and activity. (C) Body temperature was recorded by a data logger in young SARS-CoV-2-infected monkeys. Body temperature changes compared to the average body temperature during the 3 days prior to infection in each variant group were plotted. Changes in body weight (D), white blood cell counts (E), platelets (F), and CRP (G) were examined at the indicated time points. The average values in each variant are plotted. (H) CRP levels at 0-5 dpi. Data are mean ± SD and statistical analyses between groups were performed using 2-way ANOVA. *$p < 0.05$; **$p < 0.01$.,

Figure 2. Determination of viral shedding by measurements of viral loads and viral titers in nasal, and pharynx swab samples. After inoculation of SARS-CoV-2, nasal (A) and pharynx (B) swab samples were collected at the indicated time points (Wuhan: n=5, Alpha: n=3, Beta: n=3, Gamma: n=3, Delta: n=6, BA.1: n=5, and BA.2: n=3). Viral loads were determined by RT-PCR using RNA extracted from swab samples (A-B; top). Infectious viral titers in swab samples were determined by $TCID_{50}$ using VeroE6/TMPRSS2 cells (A-B; bottom). (C) The average viral loads and viral titers in each variant group are indicated. Peak viral load in each variant-infected group (C) and AUC from day 0 to day 7 in each variant group (D) are shown. Data are mean ± SD and statistical analyses between groups were performed using the Kruskal-Wallis test. *$p < 0.05$; **$p < 0.01$.

Figure 3. Pulmonary inflammation in SARS-CoV-2-infected cynomolgus macaques. Chest CT images were obtained during the experimental period (Wuhan: n=5, Alpha: n=3, Beta: n=3, Gamma: n=3, Delta: n=6, BA.1: n=5, and BA.2: n=3). Pulmonary inflammations were observed and mostly peaked at 3-5 dpi. (A) The data at peak inflammation were analyzed by AZE Virtual Place (Canon). Pneumonia non-developed animals were indicated in yellow, and 5 dpi lung image was displayed as a representative. Inflammatory areas are highlighted in red. (B) Lung inflammation area (%) was calculated by the ratio of the inflamed area volume and the lung volume excluding the bronchi using AZE Virtual Place. Data are mean ± SD.

Figure 4. Study design and prolonged examination of SARS-CoV-2-reinfected cynomolgus macaques. (A) Experimental regimens and timing of rechallenge and necropsy. SARS-CoV-2-infected CMs were rechallenged with the same or a different strain of virus at 84 days interval. (B) Monitored body temperature recorded by a data logger in young SARS-CoV-2-infected monkeys. Body temperature changes compared to the average body temperature during the 3 days prior to initial infection. The viral strain used at the initial infection is indicated at the top of the

graph. The line color in the graphs is matched with the color of the variant inoculated at the second time of infection. CRP (C) and viral load in pharynx swab (D) were examined at the indicated time points. Graphs were displayed by the group according to the virus strains used in the initial infection, with the viral strain used at the initial infection indicated at the top of each graph. The black arrow indicates the time point of the second infection. The symbol color in the graphs is matched with the color of the variant inoculated at the second infection. A blue line shows young CM, and a red line shows elderly CM. Elderly CM is indicated as "e" after the animal number.

Figure 5. Prolonged antibody responses against VOCs in SARS-CoV-2-rechallenged cynomolgus macaques. Each variant RBD-specific IgG antibodies were measured by ELISA using 1:100-diluted plasma. Antibody titers were displayed in the group by the virus strains used in the initial infection (Wuhan: n=3, Delta: n=4, BA.1: n=3, and BA.2: n=2). (A) Abs against indicated RDD and (B) Abs at 91 dpi (7 days after second infection). Data are mean ± SD and statistical analyses between groups were performed using 2-way ANOVA. *$p < 0.05$; **$p < 0.01$; ***$p < 0.001$; ****$p < 0.0001$.

Figure 6. Antigen-specific cellular immune responses.

Antigen-specific T cell responses were analyzed using PBMCs at 70 dpi (Wuhan: n=3, Delta: n=4, BA.1: n=3, and BA.2: n=2). Percentages of IFNγ^+ CD4$^+$ T cells (A), IFNγ^+ CD8$^+$ T cells (B), and CD107a$^+$ CD8$^+$ T cells (C) under the condition of 6 hr stimulation of overlapping peptide pools of spikes (Wuhan, Delta, and BA.4/BA.5) and N protein are shown. The intracellular cytokine-positive population under stimulation was calculated by subtracting the solvent control values. Data are mean ± SD and statistical analyses between groups were performed using 2-way ANOVA. *$p < 0.05$; **$p < 0.01$.

Table 1. Monkey list with characteristics

Strain	Dose	Route	Sex	Age	Weight (kg)
Wuhan	$1x10^6$ $TCID_{50}$	IT	M: 3, F:2	3 - 8	3.170 ± 1.013
Alpha	$1x10^6$ $TCID_{50}$	IT	M: 2, F:1	3 - 5	3.365 ± 0.321
Beta	$1x10^6$ $TCID_{50}$	IT	M: 2, F:1	3 - 6	3.143 ± 0.761
Gamma	$1x10^6$ $TCID_{50}$	IT	M: 2, F:1	3 - 6	3.495 ± 1.082
Delta	$1x10^6$ $TCID_{50}$	IT	M: 4, F:2	5 - 9	3.788 ± 0.872
Omicron BA.1	$1x10^6$ $TCID_{50}$	IT	M: 2, F:3	3 - 9	3.122 ± 0.452
Omicron BA.2	$1x10^6$ $TCID_{50}$	IT	M: 1, F:2	5 - 9	3.453 ± 0.533

Table 2. Re-exposure experimental study design

No.	Sex	Age	1st Virus strain	Dose	Route	2nd Virus strain	Dose	Route
#048	F	8	Wuhan	$1x10^6$ $TCID_{50}$	IT	Delta	$1x10^6$ $TCID_{50}$	IT
#058	M	3	Wuhan	$1x10^6$ $TCID_{50}$	IT	Omicron BA.1	$1x10^6$ $TCID_{50}$	IT
#045	F	23	Wuhan	$1x10^6$ $TCID_{50}$	IT	Delta	$1x10^6$ $TCID_{50}$	IT
#049	M	8	Delta	$1x10^6$ $TCID_{50}$	IT	Delta	$1x10^6$ $TCID_{50}$	IT
#057	F	9	Delta	$1x10^6$ $TCID_{50}$	IT	Omicron BA.1	$1x10^6$ $TCID_{50}$	IT
#051	M	9	Delta	$1x10^6$ $TCID_{50}$	IT	Omicron BA.1	$1x10^6$ $TCID_{50}$	IT
#047	F	26	Delta	$1x10^6$ $TCID_{50}$	IT	Delta	$1x10^6$ $TCID_{50}$	IT
#064	F	8	Omicron BA.1	$1x10^6$ $TCID_{50}$	IT	Omicron BA.1	$1x10^6$ $TCID_{50}$	IT
#066	F	9	Omicron BA.1	$1x10^6$ $TCID_{50}$	IT	Omicron BA.2	$1x10^6$ $TCID_{50}$	IT
#067	F	24	Omicron BA.1	$1x10^6$ $TCID_{50}$	IT	Omicron BA.2	$1x10^6$ $TCID_{50}$	IT
#070	F	8	Omicron BA.2	$1x10^6$ $TCID_{50}$	IT	Omicron BA.5	$1x10^6$ $TCID_{50}$	IT
#071	F	25	Omicron BA.2	$1x10^6$ $TCID_{50}$	IT	Omicron BA.5	$1x10^6$ $TCID_{50}$	IT

Editor's Summary

Investigation of SARS-CoV-2 variants using a COVID-19 monkey model reveals heterogeneous immune responses to viral infection, which may inform future vaccine strategies and public health control.

Peer review statement

Communications Biology thanks the anonymous reviewers for their contribution to the peer review of this work. Primary Handling Editors: Emily Lee and Dario Ummarino. A peer review file is available.

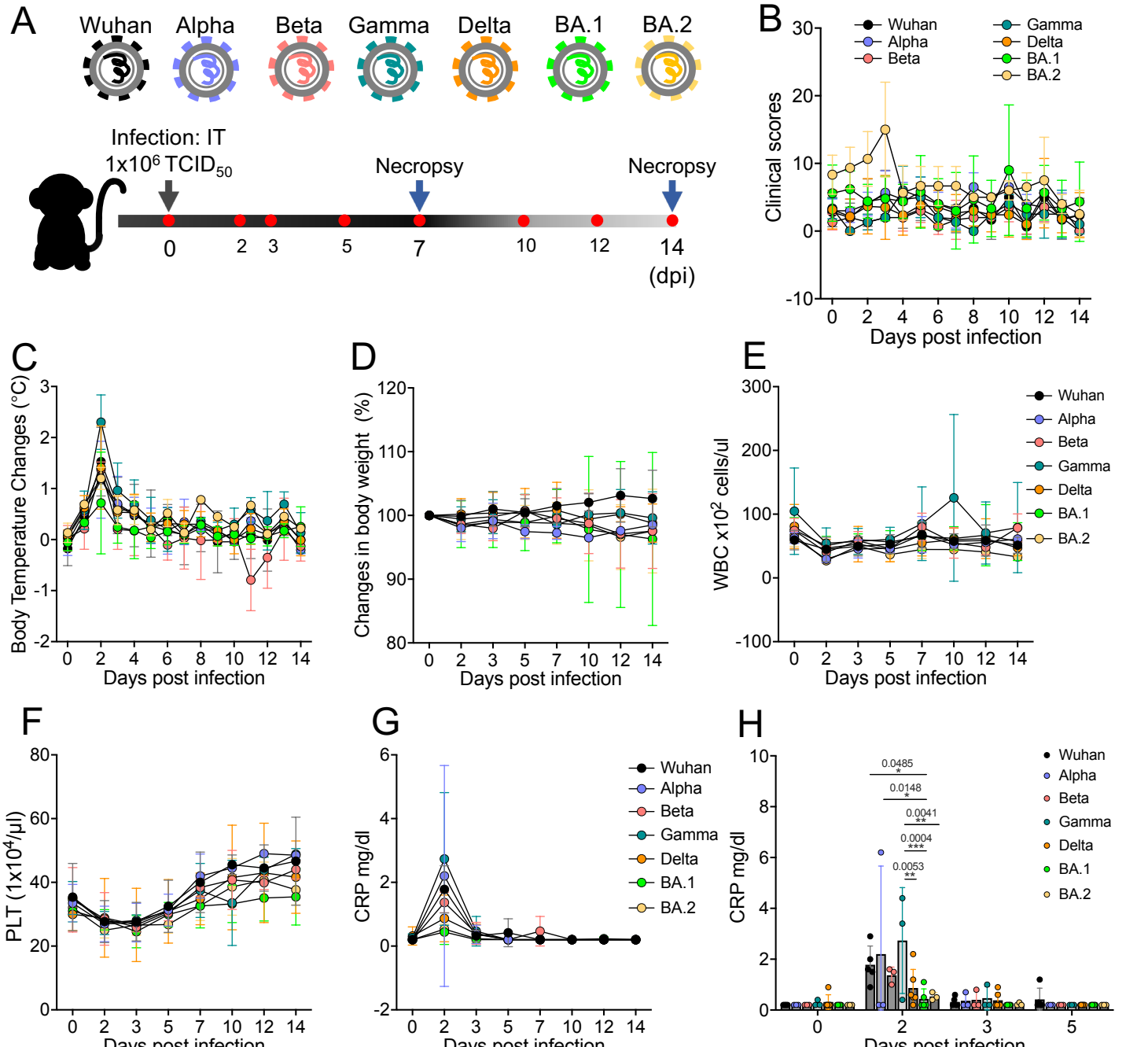
A
Wuhan
Alpha
Beta
Gamma
Delta
BA.1
BA.2
Infection: IT
1x10^6 TCID50
Necropsy
Necropsy
0
2
3
5
7
10
12
14
(dpi)
B
Clinical scores
Days post infection
C
Body Temperature Changes (°C)
Days post infection
D
Changes in body weight (%)
Days post infection
E
WBC x10^2 cells/ul
Days post infection
F
PLT (1x10^4/µl)
Days post infection
G
CRP mg/dl
Days post infection
H
CRP mg/dl
0.0485
0.0148
0.0041
0.0004
0.0053
Days post infection

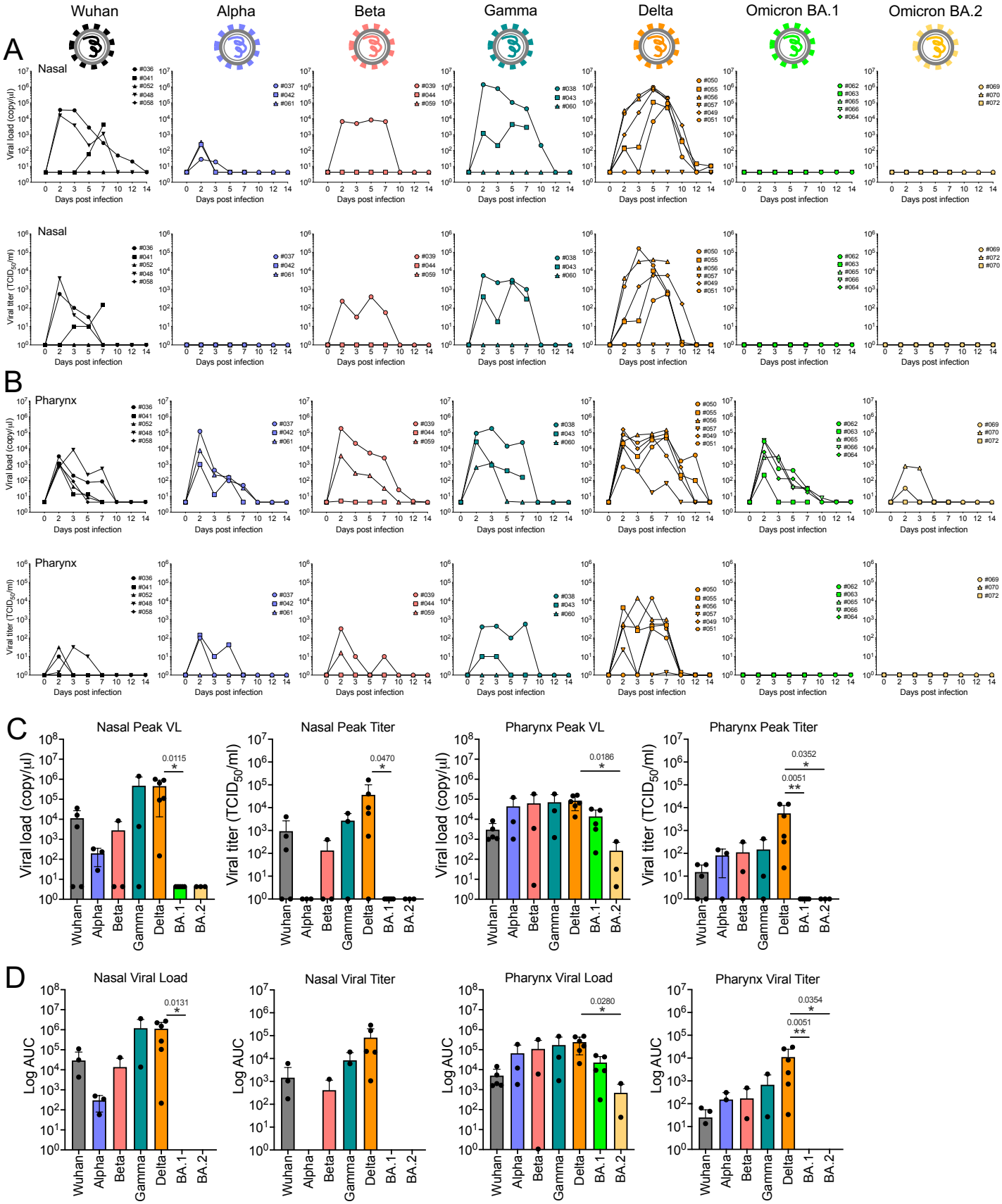
A
Wuhan
Alpha
Beta
Gamma
Delta
Omicron BA.1
Omicron BA.2
Nasal
Viral load (copy/μl)
Viral titer (TCID50/ml)
Days post infection
B
Pharynx
C
Nasal Peak VL
Nasal Peak Titer
Pharynx Peak VL
Pharynx Peak Titer
0.0115
0.0470
0.0186
0.0352
0.0051
D
Nasal Viral Load
Nasal Viral Titer
Pharynx Viral Load
Pharynx Viral Titer
Log AUC
0.0131
0.0280
0.0354
Wuhan
Alpha
Beta
Gamma
Delta
BA.1
BA.2

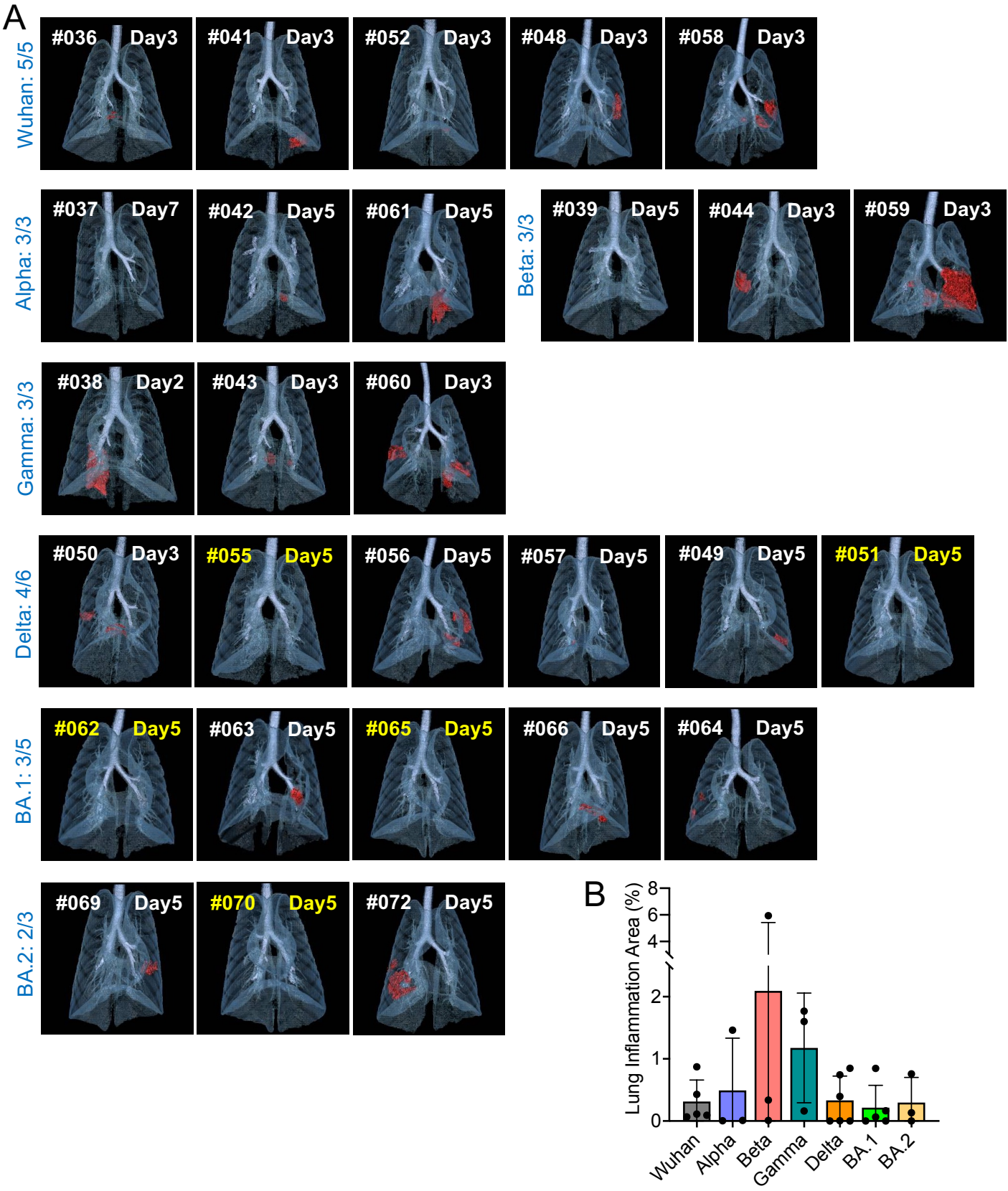
A
Wuhan: 5/5
#036 Day3
#041 Day3
#052 Day3
#048 Day3
#058 Day3
Alpha: 3/3
#037 Day7
#042 Day5
#061 Day5
Beta: 3/3
#039 Day5
#044 Day3
#059 Day3
Gamma: 3/3
#038 Day2
#043 Day3
#060 Day3
Delta: 4/6
#050 Day3
#055 Day5
#056 Day5
#057 Day5
#049 Day5
#051 Day5
BA.1: 3/5
#062 Day5
#063 Day5
#065 Day5
#066 Day5
#064 Day5
BA.2: 2/3
#069 Day5
#070 Day5
#072 Day5
B
Lung Inflammation Area (%)
8
6
4
2
1
0
Wuhan
Alpha
Beta
Gamma
Delta
BA.1
BA.2

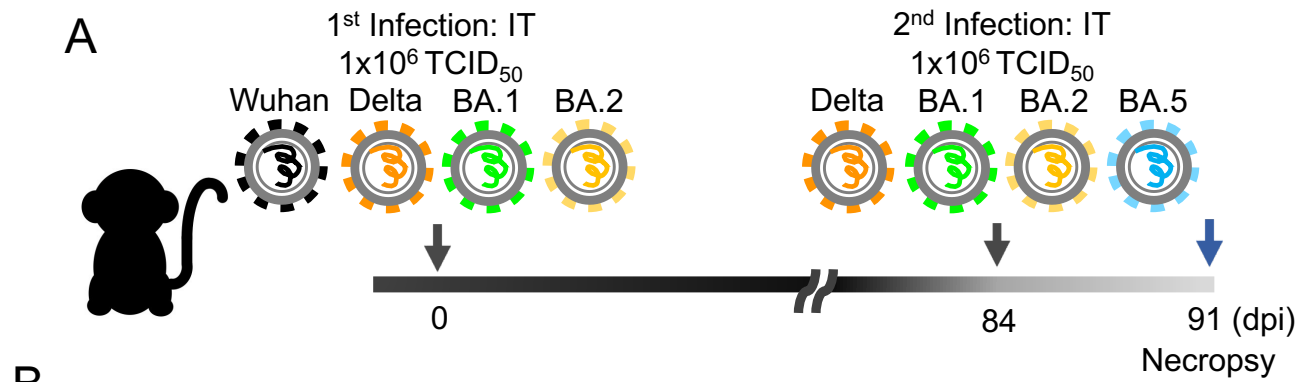
A
1st Infection: IT
1x10^6 TCID50
Wuhan
Delta
BA.1
BA.2
2nd Infection: IT
1x10^6 TCID50
Delta
BA.1
BA.2
BA.5
0
84
91 (dpi)
Necropsy

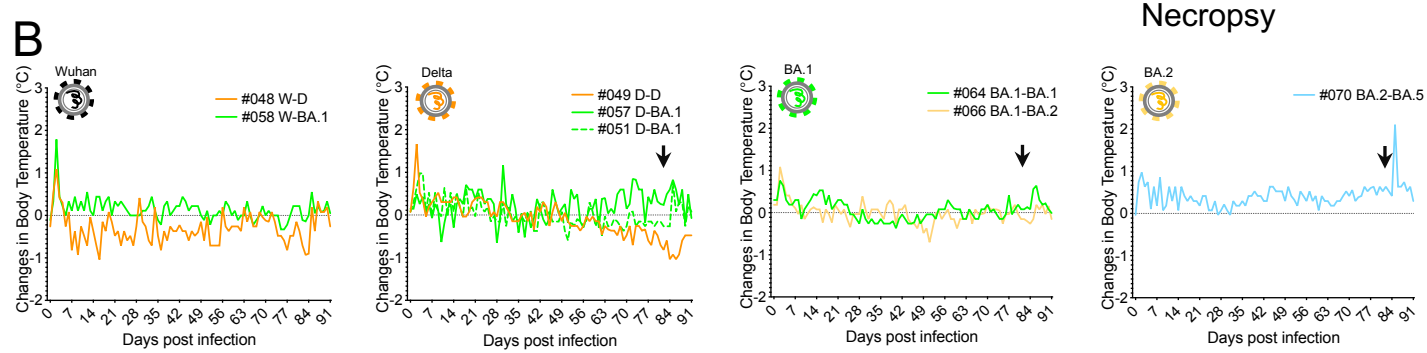
B
Wuhan
#048 W-D
#058 W-BA.1
Delta
#049 D-D
#057 D-BA.1
#051 D-BA.1
BA.1
#064 BA.1-BA.1
#066 BA.1-BA.2
BA.2
#070 BA.2-BA.5
Changes in Body Temperature (°C)
Days post infection

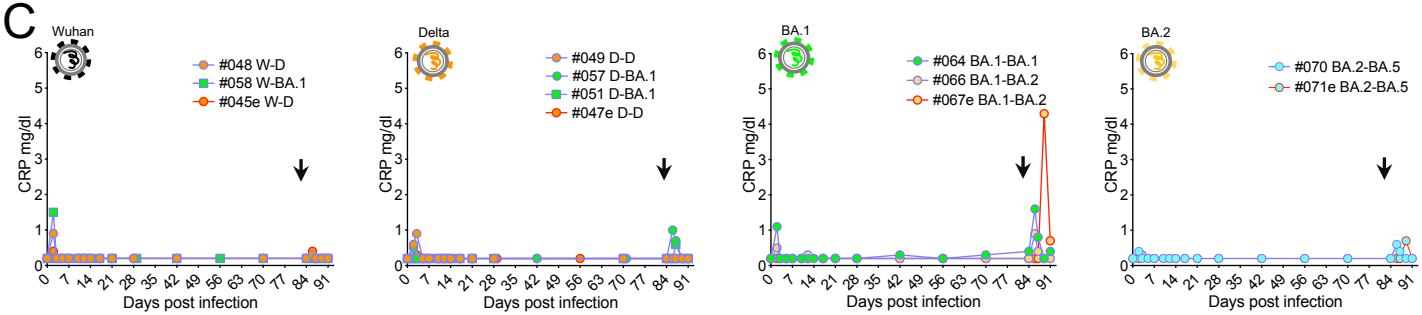
C
Wuhan
#048 W-D
#058 W-BA.1
#045e W-D
Delta
#049 D-D
#057 D-BA.1
#051 D-BA.1
#047e D-D
BA.1
#064 BA.1-BA.1
#066 BA.1-BA.2
#067e BA.1-BA.2
BA.2
#070 BA.2-BA.5
#071e BA.2-BA.5
CRP mg/dl
Days post infection

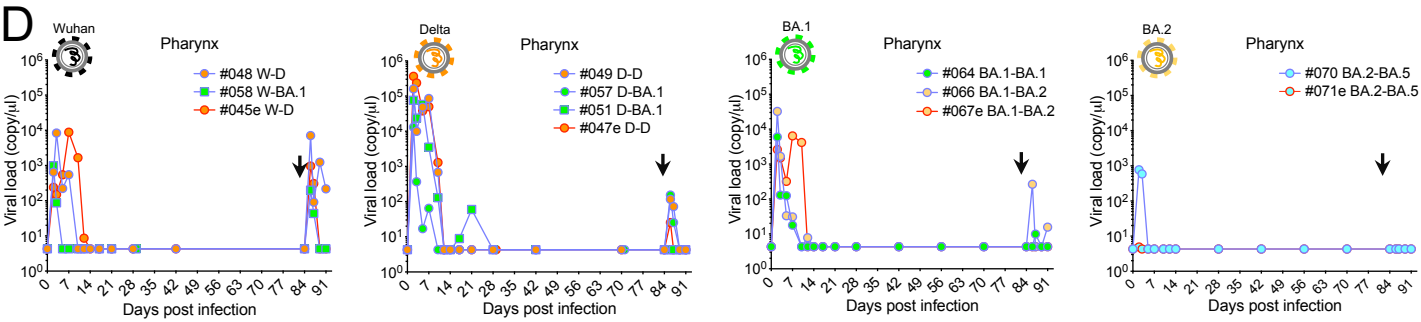
D
Wuhan
Pharynx
#048 W-D
#058 W-BA.1
#045e W-D
Delta
#049 D-D
#057 D-BA.1
#051 D-BA.1
#047e D-D
BA.1
#064 BA.1-BA.1
#066 BA.1-BA.2
#067e BA.1-BA.2
BA.2
#070 BA.2-BA.5
#071e BA.2-BA.5
Viral load (copy/μl)
Days post infection

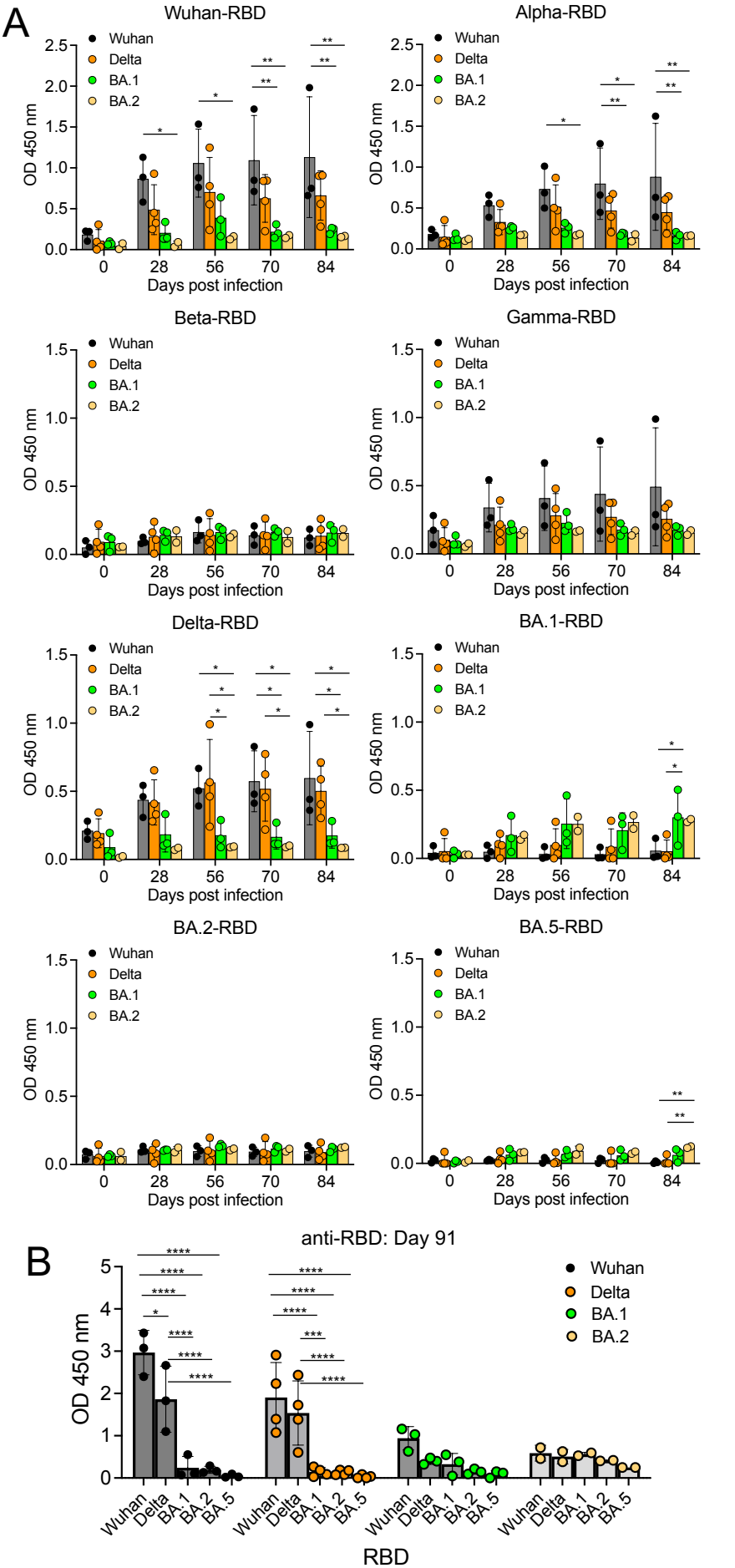
A
Wuhan-RBD
Alpha-RBD
Beta-RBD
Gamma-RBD
Delta-RBD
BA.1-RBD
BA.2-RBD
BA.5-RBD
Wuhan
Delta
BA.1
BA.2
OD 450 nm
Days post infection
0
28
56
70
84
B
anti-RBD: Day 91
OD 450 nm
Wuhan
Delta
BA.1
BA.2
BA.5
RBD